

Tetravalency and magnetic phase diagram in the heavy-fermion superconductor UPd<sub>2</sub>Al<sub>3</sub>A. Grauel, A. Böhm, H. Fischer, C. Geibel, R. Köhler, R. Modler, C. Schank, F. Steglich, and G. Weber  
*Institut für Festkörperphysik, Technische Hochschule Darmstadt, W-6100 Darmstadt, Germany*

T. Komatsubara and N. Sato

*Department of Physics, Faculty of Science, Tohoku University, Sendai 980, Japan*

(Received 14 May 1992)

Measurements of the dc susceptibility  $\chi(T)$ , dc magnetization, magnetoresistivity, and magnetostriction are utilized to delineate the magnetic  $B$ - $T$  phase diagram of the antiferromagnetically ordered ( $T_N=14$  K) heavy-fermion superconductor ( $T_c=2$  K) UPd<sub>2</sub>Al<sub>3</sub>. The single-crystal data reveal three antiferromagnetic phases for  $\mathbf{B}\perp c$ , but only one for  $\mathbf{B}\parallel c$ . The anisotropic  $\chi(T)$  in the paramagnetic state suggests a tetravalent configuration of uranium.

One of the essential open questions in heavy-fermion physics concerns the interference of antiferromagnetism and superconductivity of strongly renormalized carriers,<sup>1</sup> this question being related to the potential role of magnetic fluctuations in the Cooper pairing in heavy-fermion superconductors (HFS's).<sup>2</sup> Coexistence between HFS's and antiferromagnetism with extremely small ordered moments,  $\mu_s \sim (2-3) \times 10^{-2} \mu_B$ , was reported for URu<sub>2</sub>Si<sub>2</sub><sup>3</sup> as well as UPt<sub>3</sub>,<sup>4</sup> whereas this issue is still controversial for both CeCu<sub>2</sub>Si<sub>2</sub> (Ref. 5) and UBe<sub>13</sub> (Ref. 6). The discovery of the two homologs UM<sub>2</sub>Al<sub>3</sub>, which are antiferromagnetically ordered HFS's (Refs. 7-10) with  $T_N=4.6$  K and 14 K as well as  $T_c=1$  K and 2 K for  $M=\text{Ni}$  and Pd, respectively, has increased the number of these interesting materials. Whereas the ordered moment of UNi<sub>2</sub>Al<sub>3</sub>,  $\mu_s=0.1 \mu_B$ ,<sup>9</sup> exceeds  $\mu_s$  of URu<sub>2</sub>Si<sub>2</sub> and UPt<sub>3</sub> by a factor of 3-5 only, a  $\mu_s$  value as large as  $0.85 \mu_B$  was reported<sup>10</sup> for UPd<sub>2</sub>Al<sub>3</sub>. This latter value is of the same order as  $\mu_s$  of U<sub>2</sub>Zn<sub>17</sub> (Ref. 11) and Th- (and Pd-) doped UPt<sub>3</sub> (Ref. 4). Both systems share with UPd<sub>2</sub>Al<sub>3</sub> (Refs. 12, 13, and 10) an easy magnetic, i.e., the hexagonal, plane. On the other hand, for both UNi<sub>2</sub>Al<sub>3</sub> (Ref. 9) and tetragonal URu<sub>2</sub>Si<sub>2</sub> (Ref. 3) an easy  $c$  axis was reported.

In this paper, we address the magnetic phase diagram of UPd<sub>2</sub>Al<sub>3</sub>, based upon dc susceptibility, dc magnetization, transverse magnetoresistivity, and magnetostriction measurements on single crystals. Three different antiferromagnetic phases are found if the magnetic field is applied within the hexagonal plane ( $\mathbf{B}\perp c$ ), whereas only one magnetic transition at  $T=T_N$  can be resolved if  $\mathbf{B}\parallel c$ . A combination of susceptibility measurements on polycrystalline samples up to  $T=650$  K and on single crystals ( $T \leq 300$  K) was used to get information about the ionic configuration of uranium in UPd<sub>2</sub>Al<sub>3</sub>. A tetravalent ( $5f^2, J=4$ ) state is found to be the most likely one, similar to earlier conclusions drawn for the Ni homolog.<sup>14</sup>

The polycrystalline sample ( $T_c=2$  K) was prepared and characterized as reported in Ref. 8. Three single crystals (with  $T_c=1.4, 1.6,$  and  $1.85$  K) were grown by the Czochralski method.<sup>13</sup> All samples had the proper

CaCu<sub>5</sub>-derived PrNi<sub>2</sub>Al<sub>3</sub> structure and did not show secondary phases within the resolution of x-ray powder diffractometry and microprobe analysis (a few at. %). The single crystals (typically  $1.5 \times 1.5 \times 6$  mm<sup>3</sup>) were oriented along the [210], [110], and [100] axes, respectively. Measurements of the dc susceptibility and dc magnetization at low fields ( $B \leq 0.01$  T) were carried out in a SQUID magnetometer designed to exhibit a very low remnant field ( $\leq 10^{-7}$  T). For the high-field ( $B \leq 5.5$  T) measurements, a commercial SQUID magnetometer (Quantum design) was utilized. Measurements of the isothermal magnetoresistivity  $\Delta\rho(B)/\rho = [\rho(B) - \rho(0)]/\rho(0)$  ( $T \geq 1.5$  K,  $B \leq 8$  T), and of the isothermal magnetostriction,  $\Delta l(B)/l = [l(B) - l(0)]/l(0)$  ( $T \geq 0.05$  K,  $B \leq 8$  T), were done using standard techniques.<sup>15</sup> From an angular-dependent single-crystal measurement of the susceptibility  $\chi_1(\varphi)(\mathbf{B}\perp c)$ , no  $a/b$  anisotropy could be resolved within less than 5%.

In Fig. 1 we show the results<sup>12</sup> of the paramagnetic sus-

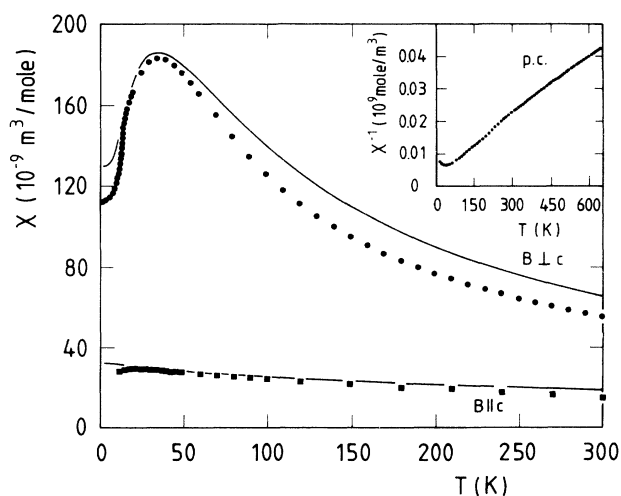


FIG. 1. dc susceptibility at  $B=10^{-2}$  T vs temperature for UPd<sub>2</sub>Al<sub>3</sub> single crystal:  $\mathbf{B}\parallel c$  (■) and  $\mathbf{B}\perp c$  (●), whereas the two solid lines are CF calculations. Inset: Inverse susceptibility vs  $T$  for a polycrystalline UPd<sub>2</sub>Al<sub>3</sub> sample up to 650 K.

ceptibility,  $\chi_{\perp}(T)$  and  $\chi_{\parallel}(T)$  ( $\mathbf{B}\parallel c$ ). Apart from a distinct anisotropy, indicating a magnetically easy basal plane, we mention the Curie-Weiss (CW) behavior found above  $T \geq 100$  K for both  $\chi_{\perp}(T)$  and  $\chi_{\parallel}(T)$ . At lower temperatures, the former exhibits a pronounced peak near  $T=35$  K, while the latter is of van Vleck type. The measurements on the polycrystalline sample reveal two linear regions in a plot  $\chi^{-1}$  vs  $T$ , the i.e., for  $100 \text{ K} \leq T \leq 300 \text{ K}$  and  $350 \text{ K} \leq T \leq 650 \text{ K}$ ; see the inset of Fig. 1. Fitting CW laws to these data, one finds an effective moment  $\mu_{\text{eff}}^{\text{low}} \approx 3.2\mu_B$  and a Weiss temperature  $\Theta_{\text{W}}^{\text{low}} = -36 \text{ K}$  for the low- $T$  region, while  $\mu_{\text{eff}}^{\text{high}} \approx 3.4\mu_B$  and  $\Theta_{\text{W}}^{\text{high}} = -123 \text{ K}$  are derived at higher  $T$ .

We ascribe these observations to the dominating effect of crystal-field (CF) splitting of the localized  $5f$  state of uranium, in accord with previous specific-heat results<sup>14</sup> and the single-crystalline susceptibility data,  $\chi_{\perp}(T)$  and  $\chi_{\parallel}(T)$ . To understand the latter, we have assumed Russel-Saunders coupling and calculated  $\chi_{\perp}(T)$  and  $\chi_{\parallel}(T)$  for various CF splittings either of the  $U^{4+}(5f^2)$ ,  $\mu_{\text{eff}} = 3.58\mu_B$  or the  $U^{3+}(5f^3)$ ,  $\mu_{\text{eff}} = 3.62\mu_B$  configuration. The  $5f^1$  state is discarded because of its small effective moment,  $\mu_{\text{eff}} = 2.54\mu_B$ . Assuming trivalent uranium, we are able to describe qualitatively the pronounced maximum in  $\chi_{\perp}(T)$ , while  $\chi_{\parallel}(T)$  is found to diverge as  $T \rightarrow 0$ , in contrast to the measured  $\chi_{\parallel}(T)$ . On the other hand, our data strongly suggest a tetravalent uranium state. This is not surprising in view of the strikingly similar anisotropy of the susceptibilities of  $\text{UPd}_2\text{Al}_3$  and  $\text{PrNi}_5$ .<sup>16</sup> In the latter compound, which crystallizes in the  $\text{CaCu}_5$  structure, the  $\text{Pr}^{3+}(4f^2)$  ions exhibit the same site symmetry as the U ions in  $\text{UPd}_2\text{Al}_3$ . The best fit to the single-crystal data in Fig. 1 was achieved with the CF-level scheme for  $U^{4+}$  displayed in Fig. 2. In these fits (solid lines in Fig. 1), intersite correlations have been accounted for by the following mean-field parameters, defined through  $\chi^{-1} = \chi_{\text{CF}}^{-1} + a^{\text{mf}}$ :  $a_{\parallel}^{\text{mf}} = 2 \times 10^7 \text{ mole/m}^3$  and  $a_{\perp}^{\text{mf}} = 2.5 \times 10^6 \text{ mole/m}^3$ , respectively. Within this CF-level scheme, the pronounced maximum of  $\chi_{\perp}(T)$  at  $T=35 \text{ K}$  is explained by different van Vleck contributions due to the two low-lying singlets and the thermal population of the excited  $\Gamma_1$  and  $\Gamma_6$  states. Similar  $\chi(T)$  maxima measured along the easy-plane/axis have also been observed for  $\text{URu}_2\text{Si}_2$  (Ref. 17) and  $\text{URu}_2\text{Si}_2$  (Ref. 18) and, for the latter compound, have likewise been attributed to a low-lying singlet belonging to the CF split  $J=4$  multiplet of  $U^{4+}$  (Ref. 19).

The present single-crystal study reveals three different

$$\begin{aligned}
 1006 \text{ K} & \text{ --- } |\Gamma_5\rangle = 0.2597 | \mp 2 \rangle + 0.9657 | \pm 4 \rangle \\
 562 \text{ K} & \text{ --- } |\Gamma_3\rangle = 1/\sqrt{2} (|1+3\rangle + |-3\rangle) \\
 152 \text{ K} & \text{ --- } |\Gamma_5\rangle = 0.9657 | \mp 2 \rangle - 0.2597 | \pm 4 \rangle \\
 102 \text{ K} & \text{ --- } |\Gamma_6\rangle = | \pm 1 \rangle \\
 33 \text{ K} & \text{ --- } |\Gamma_1\rangle = | 0 \rangle \\
 0 \text{ K} & \text{ --- } |\Gamma_4\rangle = 1/\sqrt{2} (|1+3\rangle - |-3\rangle)
 \end{aligned}$$

FIG. 2. Crystal-field level scheme for  $U^{4+}(5f^2)$  in  $\text{UPd}_2\text{Al}_3$  used to calculate the anisotropic susceptibility  $\chi(T)$  curves in Fig. 1.

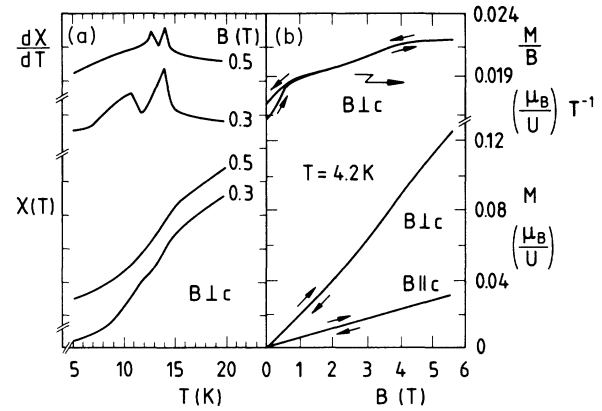


FIG. 3. (a) Susceptibility  $\chi(T)$  vs  $T$  for  $\mathbf{B}\perp c$  at  $B=0.3 \text{ T}$  and  $0.5 \text{ T}$ . Top:  $d\chi/dT$  vs  $T$  at the same magnetic fields. (b) Magnetization curves at  $T=4.2 \text{ K}$  for  $\mathbf{B}\parallel c$  and  $\mathbf{B}\perp c$ . Top curve:  $M(B)/B$  for  $\mathbf{B}\perp c$ . The hysteresis loop at  $B < 1 \text{ T}$  is lacking any remnant magnetization.

antiferromagnetic regimes (I, II, and III) in the  $B$ - $T$  diagram, if the magnetic field is applied parallel to the easy plane ( $\mathbf{B}\perp c$ ). The corresponding I-II and II-III transitions, which are *absent* for  $\mathbf{B}\parallel c$ , manifest themselves in the results of the susceptibility, magnetization, magnetoresistivity and magnetostriction [Figs. 3(a) and 3(b), and 4(a) and 4(b)] and can be used to construct the phase diagram of Fig. 5(a). The critical field for antiferromagnetic ordering,  $B_{\text{AFM}}(T)$ , i.e., the boundary between phase III and the paramagnetic state, is obtained from the Néel temperatures,  $T_N(B)$ , read off either the break slope in  $\chi_{\perp}(T)$  or the  $\lambda$ -type peak in  $d\chi_{\perp}(T)/dT$  near  $14 \text{ K}$  displayed in Fig. 3(a). For  $B \leq 5 \text{ T}$ ,  $B_{\text{AFM}}(T)$  exhibits a vertical slope. At low temperatures it assumes a value of  $\approx 18 \text{ T}$  as recently shown by high-field magnetization measurements of de Visser *et al.*;<sup>20</sup> cf. Fig. 5(b).

The transition between phases II and III is reflected by (i) a second peak, at  $T < T_N$ , in  $d\chi_{\perp}(T)/dT$  for fields  $B > 0.3 \text{ T}$  [Fig. 3(a)], (ii) an inflection point in the magnetization curve, e.g., near  $B=4 \text{ T}$  for  $T=4.2 \text{ K}$  [Fig. 3(b)], (iii) a break of slope in the transverse magnetoresistivity

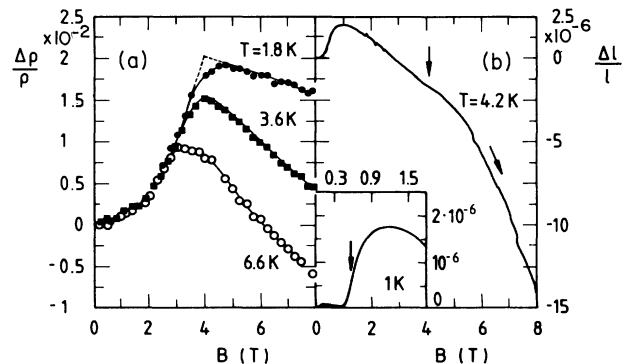


FIG. 4. (a) Isothermal transverse magnetoresistivity,  $\Delta\rho/\rho$  vs  $B$ , for different temperatures  $T < T_N$ . (b) Isothermal magnetostriction,  $\Delta l/l$  vs  $B$  at  $T=4.2 \text{ K}$  upon increasing field. Inset: low-field results at  $T=1 \text{ K}$ . Arrows mark phase transitions I-II and II-III; see text.

[Fig. 4(a)], and (iv) a very shallow “shoulder” in the magnetostriction [Fig. 4(b)]. No hysteresis effects are resolved for the II-I transition indicating that it is of second (or weakly first) order. Clearly, the transition line II-III hits (as  $B \rightarrow 0$ ) the Néel temperature, which thus behaves as a “tricritical” point in the  $B$ - $T$  plane.

Evidence for the transition from phase I to phase II (which sets in at  $T_I = 12$  K for magnetic fields  $0.01$  T  $< B \leq 0.3$  T) stems from shallow maxima in  $\chi_\perp(T)$ , respectively, sharp ones in  $d\chi_\perp(T)/dT$  [see Fig. 3(a)] as well as from a distinct increase in both  $M(B)/B$  [see the upper part of Fig. 3(b)] and  $\Delta l(B)/l$  measured along [110] [see Fig. 4(b)]. The hysteresis found for the anomaly in  $M(B)/B$  suggests that the I-II transition is of first order. The absence of a remnant magnetization seems to rule out domain-ordering effects (implying weakly ferromagnetic domain walls).<sup>21</sup> Strangely enough, no maximum can be resolved in  $\chi(T)$  for fields smaller than 0.01 T. This suggests that, for such low fields, the transition at  $T_I \approx 12$  K is of higher than second order or removed by thermal fluctuations (hinting at a critical point on the I-II phase boundary). According to the magnetostriction results, the I-II transition persists in the superconducting state [cf. the inset of Fig. 4(b)].

Our measurements prove a complex magnetization process with the easy ( $a, b$ ) plane of  $\text{UPd}_2\text{Al}_3$ , involving up to three steps depending on the temperature. According to the neutron-powder-diffraction results done at zero magnetic field by Krimmel *et al.*,<sup>10</sup> the antiferromagnetic structure of  $\text{UPd}_2\text{Al}_3$  consists of ferromagnetically ordered planes alternating along the  $c$  axis, as described by the propagation vector  $\mathbf{q} = (0, 0, 1/2)$  in reciprocal units of the chemical unit cell ( $4\pi/(\sqrt{3}a)$ ,  $4\pi/(\sqrt{3}a)$ ,  $2\pi/c$ ). In this structure, the U moments are aligned in the basal plane. In addition, an incommensurate structure was found to coexist with the  $\mathbf{q} = (0, 0, 1/2)$  ordering at temperatures slightly below  $T_N$  and to disappear only upon heating the sample up to approximately  $T = 20$  K.<sup>10</sup> No phase transition near 20 K can, however, be detected in the bulk measurements discussed in this paper. Instead, these measurements highlight a change in the magnetic structure below  $T_I \approx 12$  K (for  $B > 0.01$  T). Future neutron-diffraction experiments on single crystals have to resolve the discrepancy to the powder-diffraction data. Concerning the existence of three different “in-plane structures” as suggested by Fig. 5(a), we refer to the  $T = 0$  results of a recent local-density approximation (LDA) calculation by Sticht and Kübler:<sup>22</sup> apart from the  $\mathbf{q} = (0, 0, 1/2)$  structure, two nearly degenerate additional types of moment arrangements in the basal planes, being energetically even more favorable than the former, have been obtained. One of them is a collinear structure with  $\mathbf{q} = (1/\sqrt{3}, 0, 1/2)$  (the  $L$  point of the Brillouin zone), whereas the other one is noncollinear with  $\mathbf{q} = (1/\sqrt{3}, 1/3, 1/2)$  (the  $H$  point of the Brillouin zone). Based upon the available experimental and theoretical results, we propose that phases I, II, and III correspond to the  $\mathbf{q} = (0, 0, 1/2)$ ,  $(1/\sqrt{3}, 0, 1/2)$ , and  $(1/\sqrt{3}, 1/3, 1/2)$  structures, respectively. Partial support for this assignment derives from the field dependence of the transverse magnetoresistivity [Fig. 4(a)]: a  $B^2$  dependence of  $\Delta\rho(B)$

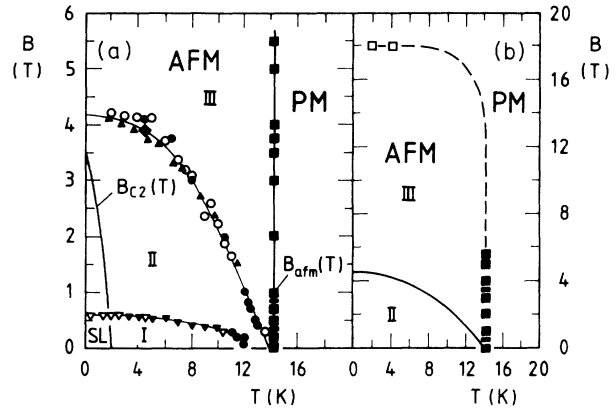


FIG. 5. (a) Magnetic phase diagram of  $\text{UPd}_2\text{Al}_3$  for  $B \parallel c$  as constructed from results of dc susceptibility  $\chi(T)$  ( $\bullet, \blacksquare$ ), magnetization  $M(B)$  ( $\circ, \blacktriangledown$ ) magnetostriction  $\Delta l(B)/l$  ( $\nabla, \blacklozenge$ ) and transverse magnetoresistivity ( $\blacktriangle$ ). The transition I-II exists above and below  $B_{c2}(T)$ . (b) Partial phase diagram including the metamagnetic transition found (Ref. 20) for  $T \leq 4.2$  K at  $B = 18$  T ( $\square$ ).

as observed in phase II is, in fact, expected for a collinear antiferromagnetic moment arrangement along the direction of the applied field.<sup>23</sup> Also, the field-induced transition to a noncollinear “in-plane” structure should cause a break in the slope of  $\Delta\rho(B)$ ,<sup>23</sup> as found at the II-III transformation. The low- $T$  magnetization demonstrates only small changes at the two low-lying transitions [Fig. 2(b)], which is not surprising for reorientation processes with the antiferromagnetic structure. By contrast, for the transition from phase III into the paramagnetic state, which takes place at  $B = 18$  T for  $T \leq 4.2$  K, a factor of 3 increase in the  $M(B)/B$  data was reported.<sup>20</sup> Neutron-diffraction experiments on single crystals are necessary to check the assignments anticipated from the present results. In particular, the existence or nonexistence of a critical point near  $T = 12$  K and  $B = 0.01$  T remains to be clarified.

In conclusion, the anisotropy of the temperature dependence of the susceptibility in the paramagnetic state of  $\text{UPd}_2\text{Al}_3$  supports strongly a tetravalent ground-state configuration of uranium. Like  $\text{URu}_2\text{Si}_2$ ,<sup>19</sup>  $\text{UPd}_2\text{Al}_3$  is identified as another heavy-fermion compound showing a singlet CF ground state within a tetravalent ionic configuration of uranium. This may imply that the ordinary (one-channel) Kondo mechanism is not sufficient to explain heavy-fermion formation in  $\text{UPd}_2\text{Al}_3$  and, therefore, more general models have to be applied.<sup>24</sup> The magnetization process within the easy magnetic plane of  $\text{UPd}_2\text{Al}_3$  passes through three phase transitions whose natures have to be unraveled by future neutron-diffraction work. Since the transition at the lowest field,  $B < 0.5$  T, remains unchanged in the superconducting state, we conclude that antiferromagnetic ordering, i.e., in both phase I and phase II, coexists with heavy-fermion superconductivity down to, at least,  $T = 50$  mK. Further on, no substantial superconductivity-induced changes in

the antiferromagnetic order are expected on the basis of the experiments presented in this paper.

We would like to thank Professor J. Kübler for stimulating discussions and Dr. A. de Visser for making avail-

able to us his high-field magnetization results prior to publication. This work was performed within the research program of the Sonderforschungsbereich 252 Darmstadt/Frankfurt/Mainz.

- <sup>1</sup>N. Grewe and F. Steglich, in *Handbook on the Physics and Chemistry of Rare Earths*, edited by K. A. Gschneidner, Jr. and L. Eyring (Elsevier, Amsterdam, 1991), Vol. 14, p. 343.
- <sup>2</sup>H. R. Ott, *Prog. Low Temp. Phys.* **11**, 215 (1987).
- <sup>3</sup>C. Broholm, J. K. Kjems, W. J. L. Buyers, P. Matthews, T. T. M. Palstra, A. A. Menowsky, and J. A. Mydosh, *Phys. Rev. Lett.* **58**, 1467 (1987).
- <sup>4</sup>G. Aeppli, E. Bucher, A. I. Goldman, G. Shirane, C. Broholm, and J. K. Kjems, *J. Magn. Magn. Mater.* **76&77**, 385 (1988).
- <sup>5</sup>F. Steglich, *J. Magn. Magn. Mater.* **100**, 186 (1991).
- <sup>6</sup>R. N. Kleiman, D. J. Bishop, H. R. Ott, Z. Fisk, and J. L. Smith, *Phys. Rev. Lett.* **64**, 1975 (1990); A. de Visser, N. H. van Dijk, J. J. M. Franse, A. Lacerda, J. Flouquet, Z. Fisk and J. L. Smith, *J. Magn. Magn. Mater.* **108**, 56 (1992).
- <sup>7</sup>C. Geibel, S. Thies, D. Kaczorowski, A. Mehner, A. Grauel, B. Seidel, U. Ahlheim, R. Helfrich, K. Petersen, C. D. Bredl, and F. Steglich, *Z. Phys. B* **83**, 305 (1991).
- <sup>8</sup>C. Geibel, C. Schank, S. Thies, H. Kitazawa, C. D. Bredl, A. Böhm, M. Rau, A. Grauel, R. Casparay, R. Helfrich, U. Ahlheim, G. Weber, and F. Steglich, *Z. Phys. B* **84**, 1 (1991).
- <sup>9</sup>A. Amato, C. Geibel, F. N. Gyax, R. H. Heffner, E. Knetsch, D. E. MacLaughlin, C. Schank, A. Schenck, F. Steglich, and M. Weber, *Z. Phys. B* **86**, 159 (1992).
- <sup>10</sup>A. Krimmel, P. Fischer, B. Roessli, H. Maletta, C. Geibel, C. Schank, A. Grauel, A. Loidl, and F. Steglich, *Z. Phys. B* **86**, 161 (1992).
- <sup>11</sup>D. E. Cox, G. Shirane, S. M. Shapiro, G. Aeppli, Z. Fisk, J. L. Smith, J. Kjems, and H. R. Ott, *Phys. Rev. B* **33**, 3614 (1986).
- <sup>12</sup>C. Geibel, U. Ahlheim, C. D. Bredl, J. Diehl, A. Grauel, R. Helfrich, H. Kitazawa, R. Köhler, R. Modler, M. Lang, C. Schank, S. Thies, F. Steglich, N. Sato, and T. Komatsubara, *Physica C* **185-189**, 2652 (1991).
- <sup>13</sup>N. Sato, T. Sakon, N. Takeda, T. Komatsubara, C. Geibel, and F. Steglich, *J. Phys. Soc. Jpn.* **61**, 32 (1992).
- <sup>14</sup>F. Steglich, U. Ahlheim, A. Böhm, C. D. Bredl, R. Caspary, C. Geibel, A. Grauel, R. Helfrich, R. Köhler, M. Lang, A. Mehner, R. Modler, C. Schank, C. Wassilew, G. Weber, W. Assmus, N. Sato, and T. Komatsubara, *Physica C* **185-189**, 379 (1991).
- <sup>15</sup>R. Köhler, Diploma thesis, Technische Hochschule Darmstadt, 1989 (unpublished); R. Modler, Diploma thesis, Technische Hochschule Darmstadt, 1992 (unpublished).
- <sup>16</sup>K. Andres, S. Darack, and H. R. Ott, *Phys. Rev. B* **19**, 5475 (1979).
- <sup>17</sup>H. R. Ott, H. Rudigier, P. Delsing, and Z. Fisk, *Phys. Rev. Lett.* **52**, 1551 (1984).
- <sup>18</sup>T. T. M. Palstra, A. A. Menowsky, J. van den Berg, A. J. Dirkmaat, P. H. Kes, G. J. Nieuwenhuys, and J. A. Mydosh, *Phys. Rev. Lett.* **55**, 2727 (1985).
- <sup>19</sup>G. J. Nieuwenhuys, *Phys. Rev. B* **35**, 5260 (1987); R. J. Radwanski, *J. Magn. Magn. Mater.* **103**, L1 (1992).
- <sup>20</sup>A. de Visser, H. Nakotte, L. T. Tai, A. A. Menowsky, S. A. M. Mentik, G. J. Nieuwenhuys, and J. A. Mydosh, *Physica B* **179**, 84 (1992).
- <sup>21</sup>See, e.g., Y. Y. Li, *Phys. Rev.* **101**, 1450 (1956).
- <sup>22</sup>J. Sticht and J. Kübler, *Z. Phys. B* **87**, 299 (1992).
- <sup>23</sup>H. Yamada and S. Takada, *J. Phys. Soc. Jpn.* **34**, 51 (1973).
- <sup>24</sup>P. Nozières and A. Blandin, *J. Phys. (Paris)* **41**, 193 (1980); D. L. Cox, *Phys. Rev. Lett.* **59**, 1243 (1987).